# Photoexcitation Cascade and Quantum-Relativistic Jets in Graphene

Cyprian Lewandowski and L. S. Levitov

Phys. Rev. Lett. **120**, 076601 — Published 14 February 2018

DOI: 10.1103/PhysRevLett.120.076601

# Photoexcitation cascade and quantum-relativistic jets in graphene

Cyprian Lewandowski, Leonid Levitov
*Department of Physics, Massachusetts Institute of Technology, Cambridge, MA 02139, USA*

In Dirac materials linear band dispersion blocks momentum-conserving interband transitions, creating a bottleneck for electron-hole pair production and carrier multiplication in the photoexcitation cascade. Here we show that the decays are unblocked and the bottleneck is relieved by subtle many-body effects in which the intermediate e-h pairs reside off-shell. The decays result from a collective behavior that cannot be accomplished by just one e-h pair but requires simultaneous coherent action by many pairs. In addition to providing a mechanism explaining existing experimental data, we predict striking characteristic signatures of the off-shell pathways such as sharp near-collinear angular distribution of secondary carriers, resembling the celebrated relativistic jets in high-energy physics. The collinear scattering enhances carrier multiplication, allowing for emission of as many as ∼10 secondary carriers per single absorbed photon.

The general question of how an excited electron partitions its energy among lower-energy excitations is central to the fields ranging from condensed matter to particle physics. One key pathway is the emission of particle-hole pairs, a process that leads to carrier multiplication in a photoexcitation cascade. Physics becomes particularly interesting in Dirac materials with linear carrier dispersion [1], where strong interactions enhance the carrier-carrier scattering whereas momentum conservation greatly restricts the phase space available for such processes and (naively) may entirely block decays (see Fig.1a) [2–4]. The competition between interactions and kinematic constraints is a foundational question for many areas in solid state and high energy physics. In models of graphene photoresponse it is usually taken for granted that energy is conserved at all times and throughout all stages of the cascade, with transitions taking place 'on-shell' [5–10]. Here we introduce the off-shell processes involving virtual states that disobey the energy-momentum relation. We argue that these processes dominate photoresponse, producing large numbers of secondary electron-hole (eh) pairs. These processes are conceptually similar to the off-shell processes in high-energy physics responsible for the formation of relativistic jets.

The dilemma faced by a photoexcited electron in a Dirac material can be summarized through the quantum-mechanical uncertainty relation. The latter permits energy non-conservation for relatively short time intervals not exceeding the inverse decay time:

$$\Delta\varepsilon \lesssim \frac{\hbar}{\tau}. \qquad (1)$$

Suppose the dependence $\tau$ vs. $\Delta\varepsilon$ is such that increasing the "offshellness" $\Delta\varepsilon$ opens up a large phase space for decays. In this case, the off-shell processes with large $\Delta\varepsilon$ will win over the processes with a smaller $\Delta\varepsilon$.

As we will see, the offshell dynamics has striking consequences for the photoexcitation cascade and, ultimately, the photoresponse. Firstly, in addition to a primary photogenerated eh pair, multiple secondary pairs will be produced through the processes of the type pictured in Fig.1b. These pairs are typically considerably softer than the primary pair, forming a broadband energy distribution analyzed below. Secondly, due to the collinear character of relevant electron-electron (ee) collision processes, the secondary pairs are preferentially emitted along the primary pair velocity direction, forming a jet-like angular distribution (see Fig.1c,e). The latter can be studied experimentally using a solid-state analog of a particle detector realized as a circular array of photocurrent de-

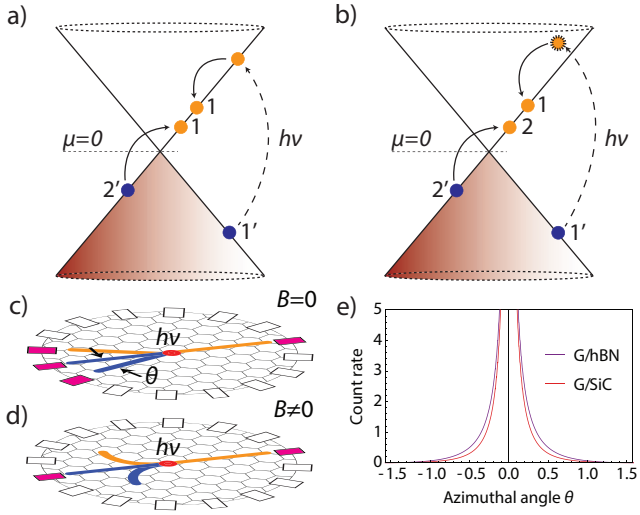


FIG. 1. a,b) Types of carrier scattering in a Dirac band. The on-shell processes (a) are subject to energy and momentum conservation, and therefore cannot trigger transitions between physical states in different linearly dispersing bands [8, 11]. This bottleneck is relieved by the off-shell processes (b) mediated by virtual states residing off the Dirac cone. This triggers collinear scattering and emission of multiple soft eh pairs with a tightly focused jet-like angular distribution. The jets can be probed as illustrated in (c,d). A photon (red dot) creates an eh jet that is detected by a group of adjacent contacts (activated contacts are shown in magenta). A weak $B$ field blocks soft pairs from reaching contacts (d), allowing for the energy distribution to be directly probed. e) Angular distribution of secondary pairs for ee interaction screened by the substrate. Parameter values used: $\kappa_{\mathrm{G/hBN}} = 3.01$, $\kappa_{\mathrm{G/SiC}} = 6.28$.

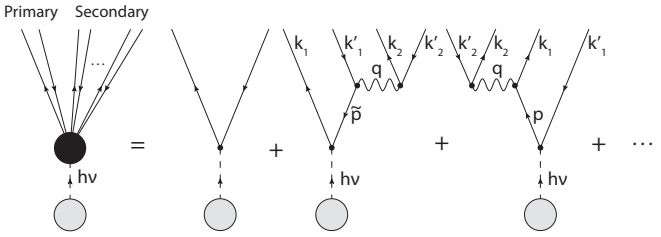


FIG. 2. Diagrammatic representation of single-photon absorption. Dashed lines describe interaction with a photon source, straight lines with arrows denote electron and hole propagators, wavy lines denote the dynamically screened Coulomb interaction, Eq.(3).

tectors [12–14], see Fig.1c. An external magnetic field that deflects the orbits of soft carriers but has little effect on the more energetic carriers (see Fig.1d). A field of strength $B$ prevents carriers with energies $\varepsilon < eBvR/2$ from reaching the detectors at a distance $R$, providing a direct probe of the energy distribution of soft pairs.

Our system is described by the Hamiltonian for $N$ species of massless Dirac particles ($N = 4$ for graphene):

$$\mathcal{H} = \sum_{i=1\ldots N} \sum_{\boldsymbol{k}} \psi^\dagger_{\boldsymbol{k},i} \left(\hbar v \boldsymbol{\sigma}\cdot\boldsymbol{k}\right) \psi_{\boldsymbol{k},i} + \mathcal{H}_{\rm ee}. \qquad (2)$$

Here the optical field is included through minimal coupling $\boldsymbol{k} \to \boldsymbol{k} - \frac{e}{\hbar c}\boldsymbol{A}$ and $\mathcal{H}_{\rm ee}$ describes ee interactions [15]. We focus on the processes in a pristine material (undoped and disorder-free), assuming high mobility, long mean free paths and, for simplicity, ignoring the effects of electron-phonon scattering. While in real materials these effects may be significant, reducing the net response, they do not alter the outcome of competition between the on-shell and off-shell ee processes.

There are several ways to develop perturbation theory for ee scattering: the weak-coupling approach uses small fine structure constant $\alpha = \frac{e^2}{\kappa\hbar v} \ll 1$, the large-$N$ approach uses as a small dimensionless coupling $1/N \ll 1$ with an RPA-screened interaction [16–19]. The latter approach (which we use below) is in principle capable of dealing with systems at strong coupling $\alpha > 1$ as long as the number of species $N$ is large enough. The resulting diagrammatics resembles that of QED, modulo replacing photon propagator by the dynamically screened Coulomb interaction [16].

A salient feature of Feynman diagrams describing the processes of secondary pair creation (see Fig.2) is the double log divergences similar to those familiar in QED and QCD [20–22]. Below we analyze excitation of eh pairs described by $\log^2$-divergent diagrams, which reflect production of infinitely many soft eh pairs. We show that in the large-$N$ framework the rate for producing $p$ pairs behaves as $N^{-p}\log^{2p}$. We tackle the multiple $\log^2$ divergences using a suitably modified QED-type approach [20], resumming the contributions with the highest powers of $\log^2$. This approach allows us to obtain a detailed picture of the cascade, including the angular distribution of secondary pairs comprising a quasirelativistic jet, and other characteristics of interest such as the energy distribution of secondary pairs. We stress that the behavior of log divergences in graphene field theory is close to that in $(3+1)$-dimensional QED [16], whereas the behavior in $(2+1)$-dimensional QED is quite different [23, 24] but is not directly relevant here.

We note that in a realistic setting the linear dispersion of Dirac bands, which is crucial for our analysis, is an asymptotic behavior valid at low enough energies. This makes the properties of soft pairs universal and largely insensitive to the details of band dispersion. This is the case, for example, for trigonal warping, which is significant away from the Dirac point, but vanishes near it [1]. Another, potentially more critical, deformation of the Dirac cone arises due to interaction-induced velocity renormalization. The latter leads to dispersion 'steepening' close to the Dirac point. This has two effects: one is further suppression of the on-shell relaxation rate, the other is a decrease in the phase-space available for particles with small offshellness. However, since these effects occur at a first-log order, they are subleading to the $\log^2$ effects analyzed below.

Photon absorption is represented diagrammatically, at the tree level, as a sum of contributions with one incoming photon leg and many outgoing particle legs, with the screened interaction (wavy lines) replacing photon propagator in the corresponding QED diagrams, as illustrated in Fig.2. The diagram with two particle legs describes creation of a primary eh pair, an on-shell process with no virtual states. Such states, present in the diagrams of higher order, are described by internal fermion lines without open ends. The higher-order diagrams describe creation of multiple secondary pairs. The wavy lines represent the dynamically screened interaction expressed through an exact polarization function as

$$\tilde{V}_{\boldsymbol{q},\omega} = \frac{V_{\boldsymbol{q}}}{1 - V_{\boldsymbol{q}}\Pi(\boldsymbol{q},\omega)}, \quad V_{\boldsymbol{q}} = \frac{2\pi e^2}{\kappa|\boldsymbol{q}|}, \qquad (3)$$

with $\boldsymbol{q}$ and $\omega$ denoting the transferred momentum and frequency, and $\kappa$ is the mean permittivity $(\kappa_1 + \kappa_2)/2$, where $\kappa_{1,2}$ characterize the material above and below graphene layer. As we will see, the polarization function needs to be introduced in order to soften the small-$q$ divergence of $V_{\boldsymbol{q}}$. We use a simple expression [11, 25],

$$\Pi(\boldsymbol{q},\omega) = -\frac{iN\boldsymbol{q}^2}{16\hbar}\frac{1}{\sqrt{\omega^2 - v^2\boldsymbol{q}^2}}, \qquad (4)$$

describing the interband eh pair excitations, $\omega > vq$.

Crucially, even a single secondary pair creation is a strongly off-shell process. Indeed, linearity of band dispersion $\varepsilon(\boldsymbol{k})$ renders the ee scattering processes obeying energy and momentum conservation to be of a strictly collinear character [2]. Collinear scattering is subject to

a phase space constraint that makes the transition rate vanish (see Fig.1a) [11]. In contrast, no phase space constraints arise for the off-shell processes (see Fig.1b), and in fact the large phase space generates the double log-divergent contributions to the transition rate. This behavior extends to all higher-order muliple pair creation processes.

Turning to the quantitative analysis, we consider the second and third diagrams pictured in Fig.2, which describe an initial photoexcited eh pair with energy and momentum positioned off-shell that excites a secondary eh pair via an interband transition. At the end all participating particles are found in the on-shell states at the Dirac cone. The transition rate for this process, within the standard Golden Rule approach, takes the form:

$$W_{0\to 1} = \frac{2\pi}{\hbar} N^2 \sum_{\boldsymbol{k}_1'+\boldsymbol{k}_2'=\boldsymbol{k}_1+\boldsymbol{k}_2} f_{\boldsymbol{k}_1'}(1-f_{\boldsymbol{k}_1}) f_{\boldsymbol{k}_2'}(1-f_{\boldsymbol{k}_2}) |\mathcal{A}|^2 \delta_{\sum \varepsilon} \tag{5}$$

Here $f_{\boldsymbol{k}}$ is the Fermi function, $h\nu$ is the absorbed photon energy (we set photon momentum equal zero), and $\delta_{\sum \varepsilon} = \delta(\varepsilon_{\boldsymbol{k}_1} + \varepsilon_{\boldsymbol{k}_2} - \varepsilon_{\boldsymbol{k}_1'} - \varepsilon_{\boldsymbol{k}_2'} - h\nu)$. The transition matrix element $\mathcal{A}$ is given by a sum of two second-order contributions, which differ by the order of the operators describing photon absorption and secondary pair creation

$$\mathcal{A} = \langle 1,2|M_{\boldsymbol{q},\omega} G(\varepsilon_{\boldsymbol{p}},\boldsymbol{p})\boldsymbol{\sigma}\boldsymbol{A} + \boldsymbol{\sigma}\boldsymbol{A} G(\varepsilon_{\tilde{\boldsymbol{p}}},\tilde{\boldsymbol{p}}) M_{\boldsymbol{q},\omega}|1',2'\rangle,$$
$$|M_{\boldsymbol{q},\omega}|^2 = |\tilde{V}_{\boldsymbol{q},\omega}|^2 \tilde{F}_{\boldsymbol{k}_2,\boldsymbol{k}_2'} F_{\boldsymbol{k}_1,\boldsymbol{k}_1'}, \tag{6}$$

where $G(\varepsilon,\boldsymbol{k})$ is the non-interacting fermion propagator, and we introduced a shorthand notation $|1,2\rangle = |\boldsymbol{k}_1,\boldsymbol{k}_2\rangle$, $|1',2'\rangle = |\boldsymbol{k}_1',\boldsymbol{k}_2'\rangle$, using unprimed and primed symbols for the states of electrons and holes (see Fig.2). For brevity, we suppress the Dirac spinor structure and incorporate the factor $ve/c$ in the definition of the optical field $\boldsymbol{A}$ (to be restored later). The quantities $F_{\boldsymbol{k},\boldsymbol{k}'}$ and $\tilde{F}_{\boldsymbol{k},\boldsymbol{k}'}$ represent the coherence factors $\langle \boldsymbol{k}'s'|\boldsymbol{k}s\rangle$ with $s=s'$ and $s\neq s'$, describing the intraband and interband transitions, respectively [26]. The two terms in Eq.(6) describe the processes in which photon absorption is followed by a pair creation, and vice versa. The virtual states in the two contributions, Eq.(6), are characterized by the off-shell energy values: $\varepsilon_{\boldsymbol{p}} = h\nu + \varepsilon_{\boldsymbol{k}_1'}$, $\boldsymbol{p} = \boldsymbol{k}_1'$ and $\varepsilon_{\tilde{\boldsymbol{p}}} = \varepsilon_{\boldsymbol{k}_1} - h\nu$, $\tilde{\boldsymbol{p}} = \boldsymbol{k}_1$ (we use notations from Fig.2).

As we show below, the typical energy of secondary pairs $\omega$ is much smaller than the photoexcitation energy $h\nu$. Anticipating this result it is convenient to factorize the transition rate, expressing it through the spectral function of pair excitations. Following the standard route [27] we first split the energy delta function in Eq.(5):

$$\delta_{\sum \varepsilon} = \int_{-\infty}^{\infty} \mathrm{d}\omega \delta(\varepsilon_{\boldsymbol{k}_1} - \varepsilon_{\boldsymbol{k}_1'} - h\nu + \omega)\delta(\varepsilon_{\boldsymbol{k}_2} - \varepsilon_{\boldsymbol{k}_2'} - \omega)$$

Next, using the identity $f_{\boldsymbol{k}'}(1-f_{\boldsymbol{k}}) = (f_{\boldsymbol{k}'} - f_{\boldsymbol{k}})(N_{\varepsilon_{\boldsymbol{k}}-\varepsilon_{\boldsymbol{k}'}}+1)$, where $N_\omega = \frac{1}{e^{\beta\omega}-1}$ is the Bose function taken at the electron temperature, we rewrite the sum of $(f_{\boldsymbol{k}_2'} - f_{\boldsymbol{k}_2})\delta(\varepsilon_{\boldsymbol{k}_2} - \varepsilon_{\boldsymbol{k}_2'} - \omega)$ as (denoting $\boldsymbol{q} = \boldsymbol{k}_2 - \boldsymbol{k}_2'$)

$$\mathrm{Im}\,\Pi(\boldsymbol{q},\omega) = -N\pi \sum_{\boldsymbol{k}_2} \tilde{F}_{\boldsymbol{k}_2,\boldsymbol{k}_2'}(f_{\boldsymbol{k}_2'} - f_{\boldsymbol{k}_2})\delta(\varepsilon_{\boldsymbol{k}_2} - \varepsilon_{\boldsymbol{k}_2'} - \omega),$$

a relation that follows from the definition of the polarization function [25, 28]. This yields a more compact expression for the transition rate:

$$W_{0\to 1} = -\frac{2N}{\hbar} \sum_{\boldsymbol{k}_1,\boldsymbol{k}_1',\boldsymbol{q},\omega} f_{\boldsymbol{k}_1'}(1-f_{\boldsymbol{k}_1})(N_\omega+1)|\mathcal{A}'|^2 \tag{7}$$
$$\times\ \mathrm{Im}\,\Pi(\boldsymbol{q},\omega) F_{\boldsymbol{k}_1,\boldsymbol{k}_1'} |\tilde{V}_{\boldsymbol{q},\omega}|^2 \delta_{\boldsymbol{k}_1',\boldsymbol{k}_1+\boldsymbol{q}} \delta(\varepsilon_{\boldsymbol{k}_1} - \varepsilon_{\boldsymbol{k}_1'} - h\nu + \omega)$$

where $\omega$ and $\boldsymbol{q}$ are the energy and momentum of the soft pair. Here we introduced the quantity

$$\mathcal{A}' = \langle 1|G(\varepsilon_{\boldsymbol{p}},\boldsymbol{p})\boldsymbol{\sigma}\boldsymbol{A} + \boldsymbol{\sigma}\boldsymbol{A} G(\varepsilon_{\tilde{\boldsymbol{p}}},\tilde{\boldsymbol{p}})|1'\rangle \tag{8}$$

which represents the transition matrix element for the primary ('hard') pair, factoring out the contribution of the soft pair as described above (we again use a shorthand notation for the electron and hole states $|\boldsymbol{k}_1\rangle$ and $|\boldsymbol{k}_1'\rangle$ in Fig.1c, for brevity suppressing the spin structure).

At this stage it is convenient to approximate the Green's functions of fermions in the virtual states [$G(\varepsilon_{\boldsymbol{p}},\boldsymbol{p})$ and $G(\varepsilon_{\tilde{\boldsymbol{p}}},\tilde{\boldsymbol{p}})$ in Eq.(8)] by expanding in the small frequency $\omega$ and momentum $\boldsymbol{q}$ transferred to the soft pair. This is done by writing $\varepsilon_{\boldsymbol{p}} = \varepsilon_{\boldsymbol{k}_1} + \omega$, $\boldsymbol{p} = \boldsymbol{k}_1 + \boldsymbol{q}$ and $\varepsilon_{\tilde{p}} = \varepsilon_{\boldsymbol{k}_1'} - \omega$, $\tilde{\boldsymbol{p}} = \boldsymbol{k}_1' - \boldsymbol{q}$ and expanding in $\omega$ and $\boldsymbol{q}$. The approximation that uses the softness of the secondary pair as a small parameter is known as the 'eikonal approximation', since at small $\omega$ and $\boldsymbol{q}$ only the phase of the fermion wavefunction varies but not the spinor part. We obtain simple expressions

$$G(\varepsilon_{\boldsymbol{p}},\boldsymbol{p}) \approx \frac{-1}{\omega + vq_\parallel}, \quad G(\varepsilon_{\tilde{\boldsymbol{p}}},\tilde{\boldsymbol{p}}) \approx \frac{1}{\omega - vq_\parallel}, \tag{9}$$

where $q_\parallel$ is the component of $\boldsymbol{q}$ parallel to $\boldsymbol{k}_1$. We note parenthetically that the denominators in Eq.(9) do not vanish since the soft pairs obey $|\omega| > v|\boldsymbol{q}|$. The matrix element $\mathcal{A}'$ is then reduced to

$$\mathcal{A}' \approx \frac{2vq_\parallel \langle 1|\boldsymbol{\sigma}\boldsymbol{A}|1'\rangle}{\omega^2 - v^2 q_\parallel^2}. \tag{10}$$

After plugging it in Eq.(7), the quantity $W_{0\to 1}$ becomes

$$W_{0\to 1} = -\frac{8N}{\hbar} \sum_{\boldsymbol{k}_1,\boldsymbol{q}} |\tilde{V}_{\boldsymbol{q},\omega}|^2\ \mathrm{Im}\,\Pi(\boldsymbol{q},\omega) \left| \frac{vq_\parallel \langle 1|\boldsymbol{\sigma}\boldsymbol{A}|1'\rangle}{\omega^2 - v^2 q_\parallel^2} \right|^2, \tag{11}$$

where $\omega = h\nu - 2v|\boldsymbol{k}_1| - vq_\parallel$ and, since $T \ll h\nu$, we set $N_\omega = 0$. To arrive at Eq.(11) we approximated the intraband coherence factor by unity, since $F_{\boldsymbol{k}_1,\boldsymbol{k}_1+\boldsymbol{q}} \approx 1$ in the soft-pair limit $q \ll k_1$. The interband coherence

factor $F$ has been included in the soft pair spectral function through the factorization procedure outlined above. Finite temperature does not appear in Eq.(11) explicitly, however it will control the broadening of the Dirac point, serving as a cutoff for infrared divergences that will be discussed shortly.

The most interesting property of the transition rate $W_{0\to1}$ is the double log divergence originating from the collinear nature of ee scattering. The divergence arises due singular behavior of the quantities in Eq.(11) upon integration upon the soft-pair momentum $\boldsymbol{q}$. In that, one log divergence arises from the integral over the length $|\boldsymbol{q}|$, the other log comes from integration over the angle between $\boldsymbol{q}$ and $\boldsymbol{k}_1$. For a quantitative estimate we evaluate the double log contribution at leading order in $1/N$, which can be done by approximating $\tilde{V}_{\boldsymbol{q},\omega} \approx -1/\Pi(\boldsymbol{q},\omega)$. After integrating over $\boldsymbol{q}$ and $\boldsymbol{k}_1$, and factoring out $W_{\text{on-shell}}$, the transition rate for the on-shell diagram in Fig.1e, the transition rate $W_{0\to1}$ becomes

$$\frac{W_{0\to1}}{W_{\text{on-shell}}} \approx \frac{8}{N\pi^2}\left(\ln\frac{\varepsilon_>}{\varepsilon_<}\right)^2, \quad W_{\text{on-shell}} = \frac{e^2\boldsymbol{A}^2 h\nu}{c^2}\frac{N}{8}, \tag{12}$$

where $\approx$ indicates that we suppressed an additive constant [15]. Here the UV cutoff $\varepsilon_>$ is of order $h\nu/2$ (energy of an excited electron immediately after photon absorption). The IR cutoff $\varepsilon_<$ is set by the width of the Dirac point, controlled by temperature or disorder, whichever is larger. The $\log^2$ divergence in Eq.(12) is a direct consequence of linear dispersion, arising from soft secondary pairs which are near-collinear with respect to the primary pair direction.

The double-log divergence in the transition rate is reminiscent of the double-log divergences familiar from QCD or QED calculations. This can be seen e.g. by comparing to soft Bremsstrahlung in QED [22], and noting that the double logs arise in an identical manner in both cases, with one log originating from an integral over momentum magnitude and the other from angular integration. As in QED, the IR double log divergence means that the secondary pairs are much softer than the primary pair, vindicating our eikonal approximation.

We parenthetically note that dynamical screening, Eq.(3), is crucial for our analysis. Had an unscreened Coulomb interaction $V_{\boldsymbol{q}}$ been used, the transition rate would have been IR divergent as a power law rather than as $\log^2$. This is in line with the argument that the perturbation series for Dirac semimetals should be carried out in powers of a screened interaction rather than the bare one [19]. This is in contrast to QED, where double log divergences arise from perturbation theory in bare coupling.

Motivated by the resemblance to QED, the higher-order contributions of the form $N^{-n}\log^{2n}$ can be analyzed by a Sudakov-like resummation scheme of leading double-log divergent diagrams. These diagrams describe primary pair creation followed by emission of multiple secondary pairs in analogy to 'hard' scattering processes in QED accompanied by emission of soft photons. There are soft eh pairs of two distinct types emitted, respectively, by the hard electron and the hard hole (the corresponding digrams are pictured in Fig.2). For each type, in the limit of the emitted pairs being independent of one another and assuming no mutual phase-space blocking, the probability distribution is Poissonian [22],

$$p_n = \frac{\tilde{\lambda}^n}{n!}e^{-\tilde{\lambda}}, \quad \tilde{\lambda} = \frac{4}{N\pi^2}\left(\ln\frac{\varepsilon_>}{\varepsilon_<}\right)^2. \tag{13}$$

The value $\tilde{\lambda}$ is a half of the total single-pair emission rate given in Eq.(12). Combining two identical Poisson distributions gives a Poisson distribution with a double rate [15]

$$\frac{W_{0\to n}}{W_{\text{on-shell}}} = \frac{\lambda^n e^{-\lambda}}{n!}, \quad \lambda = 2\tilde{\lambda} = \frac{8}{N\pi^2}\left(\ln\frac{\varepsilon_>}{\varepsilon_<}\right)^2. \tag{14}$$

The mean number of secondary pairs $\langle N_{\text{sec}}\rangle = \lambda$ goes as $\log^2$ and hence can be much greater than unity. As an illustration, a $h\nu = 1$eV photon absorbed in graphene creates $\sim 4$ pairs at room temperature and $\sim 7$ pairs at 77K, where the dependence on photon energy and temperature enter through $\varepsilon_>$ ad $\varepsilon_<$, respectively. The mean number of pairs $\langle N_{\text{sec}}\rangle$ slowly increases as temperature decreases, reaching $\sim 20$ pairs at 1K [15].

One interesting implication of our analysis is that the process in which no soft pairs are emitted has a vanishing rate. Indeed, $W_{0\to0}$ vanishes in the limit $\varepsilon_< \to 0$. To interpret this result we note that the sum of all partial rates equals the bare on-shell rate: $\sum_{n=0}^{\infty} W_{0\to n} = W_{\text{on-shell}}$. This means that massive emission of soft pairs does not alter the net photon absorption probability. At the same time the absorbed photon energy is redistributed among a large number of secondary eh pairs (carrier multiplication).

As discussed in the Supplement [15], massive production of soft near-collinear pairs occurs in the direction of the primary excitation, forming a pair of jets. The jets are manifest in a sharp angular distribution of emitted pairs with singularities at $\theta = 0, \pi$ (see Fig.1c). They are also characterized by a broad energy distribution with a tail at low energies, $\propto \omega^{-1}$, confirming our assumption about the dominant role of soft pairs.

In summary, the off-shell pathways unblock kinematic constraints for collinear scattering in a Dirac band, allowing a large number of secondary pairs to be produced as the photogenerated carriers cascade down in energy. The angular distribution of secondary pairs is sharply peaked along the primary pair velocity, representing a condensed-matter analog of relativistic jets familiar from high-energy physics. As discussed above, the jets can be directly probed using a solid-state equivalent of particle detectors (Fig.1c,d). Formation of jets is corroborated by recent experimental studies of Auger scattering

processes [29, 30], which indicate that at weak electron-phonon coupling the collinear scattering processes dominate the relaxation pathways of photoexcited carriers.

We acknowledge support of the Center for Integrated Quantum Materials (CIQM) under NSF award DMR-1231319.

[1] A. H. Castro Neto, F. Guinea, N. M. R. Peres, K. S. Novoselov, and A. K. Geim, Rev. Mod. Phys. **81**, 109 (2009).
[2] J. González, F. Guinea, and M. A. H. Vozmediano, Phys. Rev. Lett. **77**, 3589 (1996).
[3] F. Rana, Phys. Rev. B **76**, 155431 (2007).
[4] M. S. Foster and I. L. Aleiner, Phys. Rev. B **79**, 085415 (2009).
[5] T. Winzer and E. Malić, Phys. Rev. B **85**, 241404 (2012).
[6] D. Brida, A. Tomadin, C. Manzoni, Y. J. Kim, A. Lombardo, S. Milana, R. R. Nair, K. S. Novoselov, A. C. Ferrari, G. Cerullo, and M. Polini, Nature Communications **4**, 1987 (2013).
[7] A. Tomadin, D. Brida, G. Cerullo, A. C. Ferrari, and M. Polini, Phys. Rev. B **88**, 035430 (2013).
[8] J. C. W. Song, K. J. Tielrooij, F. H. L. Koppens, and L. S. Levitov, Phys. Rev. B **87**, 155429 (2013).
[9] J. C. W. Song and L. S. Levitov, Journal of Physics: Condensed Matter **27**, 164201 (2015).
[10] M. Trushin, Phys. Rev. B **94**, 205306 (2016).
[11] M. Schütt, P. M. Ostrovsky, I. V. Gornyi, and A. D. Mirlin, Phys. Rev. B **83**, 155441 (2011).
[12] D. Sun, G. Aivazian, A. M. Jones, J. S. Ross, W. Yao, D. Cobden, and X. Xu, Nat Nano **7**, 114 (2012).
[13] M. W. Graham, S.-F. Shi, D. C. Ralph, J. Park, and P. L. McEuen, Nat Phys **9**, 103 (2013).
[14] K. J. Tielrooij, M. Massicotte, L. Piatkowski, A. Woessner, Q. Ma, P. Jarillo-Herrero, N. F. van Hulst, and F. H. L. Koppens, Journal of Physics: Condensed Matter **27**, 164207 (2015).
[15] See Supplemental Material at [URL will be inserted by publisher] where additional details are discussed.
[16] J. González, F. Guinea, and M. A. H. Vozmediano, Phys. Rev. B **59**, R2474 (1999).
[17] D. T. Son, Phys. Rev. B **75**, 235423 (2007).
[18] E. Barnes, E. H. Hwang, R. E. Throckmorton, and S. Das Sarma, Phys. Rev. B **89**, 235431 (2014).
[19] J. Hofmann, E. Barnes, and S. Das Sarma, Phys. Rev. Lett. **113**, 105502 (2014).
[20] V. N. Gribov and L. N. Lipatov, Sov. J. Nucl. Phys. **15**, 438 (1972), [Yad. Fiz.15,781(1972)].
[21] Y. Dokshitzer, *Basics of perturbative QCD* (Editions Frontières, Gif-sur-Yvette, France, 1991).
[22] M. E. Peskin and D. V. Schroeder, *An Introduction to quantum field theory* (Westview Press, 1995) Chap. 6.
[23] R. Jackiw and S. Templeton, Phys. Rev. D **23**, 2291 (1981).
[24] D. Sen, Phys. Rev. D **41**, 1227 (1990).
[25] E. H. Hwang and S. Das Sarma, Phys. Rev. B **75**, 205418 (2007).
[26] T. Ando, J. Phys. Soc. Jpn. **75**, 074716 (2006).
[27] G. F. Giuliani and J. J. Quinn, Phys. Rev. B **26**, 4421 (1982).
[28] B. Wunsch, T. Stauber, F. Sols, and F. Guinea, New Journal of Physics **8**, 318 (2006).
[29] J. C. König-Otto, M. Mittendorff, T. Winzer, F. Kadi, E. Malic, A. Knorr, C. Berger, W. A. de Heer, A. Pashkin, H. Schneider, M. Helm, and S. Winnerl, Phys. Rev. Lett. **117**, 087401 (2016).
[30] T. Winzer, R. Jago, and E. Malic, Phys. Rev. B **94**, 235430 (2016).